PHILOSOPHICAL TRANSACTIONS OF THE ROYAL SOCIETY A MATHEMATICAL, PHYSICAL & ENGINEERING SCIENCES

Evaporative lithographic patterning of binary colloidal films

Daniel J. Harris, Jacinta C. Conrad and Jennifer A. Lewis

Phil. Trans. R. Soc. A 2009 **367**, 5157-5165
doi: 10.1098/rsta.2009.0157

PHILOSOPHICAL TRANSACTIONS OF THE ROYAL SOCIETY A

Phil. Trans. R. Soc. A (2009) **367**, 5157–5165
doi:10.1098/rsta.2009.0157

Evaporative lithographic patterning of binary colloidal films

By Daniel J. Harris, Jacinta C. Conrad and Jennifer A. Lewis*

Department of Materials Science and Engineering and Frederick Seitz Materials Research Laboratory, University of Illinois at Urbana-Champaign, Urbana, IL 61801, USA

Evaporative lithography offers a promising new route for patterning a broad array of soft materials. In this approach, a mask is placed above a drying film to create regions of free and hindered evaporation, which drive fluid convection and entrained particles to regions of highest evaporative flux. We show that binary colloidal films exhibit remarkable pattern formation when subjected to a periodic evaporative landscape during drying.

Keywords: drying; colloids; lithography; films

1. Introduction

The ability to pattern colloidal films is of growing importance for novel coatings (Martinez & Lewis 2002; Harris *et al.* 2007; Harris & Lewis 2008), metallized ceramic layers (Masuda *et al.* 2003) and even high throughput DNA screening (Jing *et al.* 1998). Most patterning approaches guide colloidal assembly either through chemical (Aizenberg *et al.* 2000; Lee *et al.* 2002; Zheng *et al.* 2002) or topographical (van Blaaderen *et al.* 1997; Lin *et al.* 2000; Yin *et al.* 2001; Lee *et al.* 2004) modification of the underlying substrate or by application of an external field (Richetti *et al.* 1984; Hayward *et al.* 2000; Ristenpart *et al.* 2003, 2004; Bhatt *et al.* 2005; Velev & Bhatt 2006). However, those approaches often require multiple processing steps, while only guiding the deposition of a few particle layers. To overcome such limitations, we recently introduced a new route for patterning colloidal films, known as evaporative lithography (Harris *et al.* 2007).

Our approach builds on prior observations of fluid flow and particle migration in freely evaporating aqueous (Chiu & Cima 1993; Deegan *et al.* 1997, 2000; Routh & Russel 1998; Deegan 2000; Shmuylovich *et al.* 2002; Hu & Larson 2005*a*; Smalyukh *et al.* 2006) and organic (Berg *et al.* 1966; Savino *et al.* 2002; Hu & Larson 2005*b*, 2006; Girard *et al.* 2006; Ristenpart *et al.* 2007) droplets. In aqueous colloidal droplets, contact line pinning and higher evaporation rates at the edge of the drop lead to the outward flow of fluid and entrained particles, yielding the well-known 'coffee-ring' effect (Deegan *et al.* 1997). By contrast, in freely evaporating, non-aqueous drops, the outward flow of fluid and entrained particles is reversed due to Marangoni stresses (Hu & Larson 2006). Evaporative cooling

*Author for correspondence (jalewis@uiuc.edu).

One contribution of 12 to a Discussion Meeting Issue 'Colloids, grains and dense suspensions: under flow and under arrest'.

and inefficient heat transfer through the drop induce a temperature gradient, which in turn leads to an inverse gradient in surface tension across the drop's surface such that the temperature is lowest and the surface tension is highest at the centre of the drop. Recirculating flows develop as fluid is transported from regions of lowest surface tension to regions of highest surface tension. Unlike aqueous colloidal films, the majority of the particles are deposited in the centre of the drop, rather than at its edge.

By introducing a periodically varying evaporative landscape above unary colloidal films, we have reported direct (Harris *et al.* 2007) and inverse (Harris & Lewis 2008) pattern formation during drying of aqueous and non-aqueous systems, respectively. In this paper, we investigate pattern formation in binary colloidal mixtures that are suspended in water. During evaporative lithography, both particle populations are entrained within the fluid and migrate to regions of highest evaporative flux. The observed pattern formation can be tuned by varying the mask design, mixture composition and particle size ratio.

Below, we review the fundamental phenomena that give rise to pattern formation during evaporative lithography in §2. In §3, we describe the pattern formation observed in binary colloidal films composed of microsphere–nanoparticle mixtures that are subjected to a periodically varying evaporative landscape during drying. Finally, we provide suggestions for other areas of exploration using this nascent approach in §4.

2. Evaporative lithography: a brief review

Evaporative lithographic patterning of unary colloidal suspensions has been demonstrated for aqueous (Harris *et al.* 2007) and non-aqueous systems (Harris & Lewis 2008). In prior efforts, a mask composed of a periodic array of holes of diameter d_h and pitch P was placed above the drying suspension, as shown in figure 1*a*. A finite separation distance was maintained between the mask and underlying droplet (or film), as shown in figure 1*b*, where h_g defines the initial gap height between the mask and underlying film. As drying proceeds, the film experiences an evaporative landscape that is modulated by the mask above it.

Through finite-element modelling (FEM), we showed that this evaporative landscape varies periodically in accord with the mask design. The maximum evaporative flux, J_{max}, occurs under the open regions of the mask, whereas the minimum evaporative flux, J_{min}, approaches zero under the masked regions of the drying film (see figure 2; Harris *et al.* 2007). Although fluid evaporation is higher in the open regions, surface tension acts to keep the drying film flat. In aqueous systems, fluid flows towards the evaporating regions to compensate for the fluid loss; concurrently, entrained particles accumulate beneath the open regions, as shown in figure 1*c*. When the difference in evaporative flux, $\Delta J = J_{max} - J_{min}$, is normalized by that observed for a freely evaporating film J_{free}, we find that $\Delta J/J_{free}$ must exceed unity to induce significant pattern formation. Importantly, evaporation is strongly suppressed under the masked regions when either h_g is small or P is large, thereby yielding $\Delta J/J_{free} > 1$. In prior work, we identified a critical value of the gap height-to-pitch ratio, h_g^*/P, of 0.3, below which pattern formation occurs (Harris *et al.* 2007).

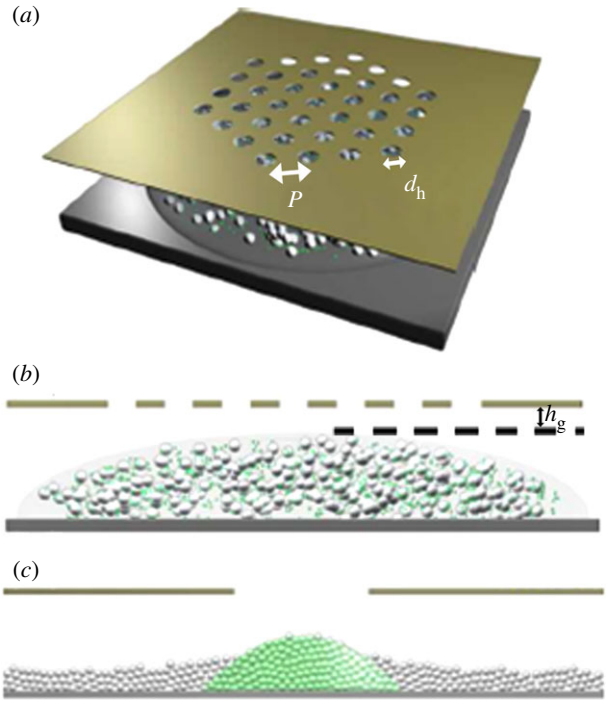

Figure 1. Schematic illustration of evaporative lithographic patterning. (*a*) Top view of a binary colloidal mixture drying beneath a patterned mask that contains a hexagonal array of holes with diameter d_h and pitch, or centre-to-centre spacing P, (*b*) side view of the initial gap height h_g between the mask and underlying binary colloidal suspension and (*c*) magnified side view of resulting binary film produced from an initial suspension that contains a high concentration of colloidal microspheres (depicted as grey spheres) and a dilute concentration of nanoparticles (depicted as green spheres). (Note: the dried film consists of a periodic array of discrete nanoparticle features (shaded green in (*c*)) embedded within a continuous colloidal network.)

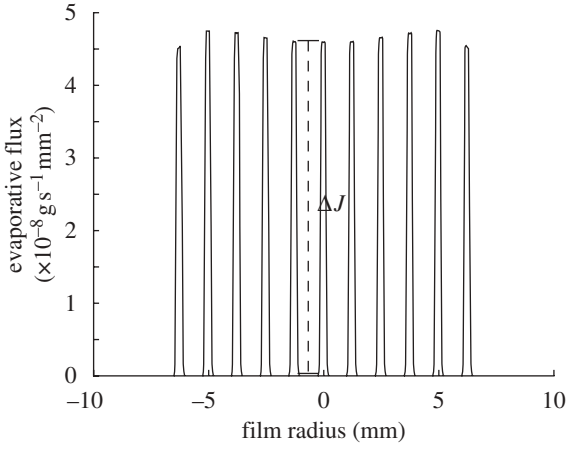

Figure 2. Calculated evaporation profile of a colloidal film dried under a mask with $d_h = 250\,\mu m$, $P = 5d_h$ and $h_g \approx 150\,\mu m$. Adapted from Harris *et al.* (2007).

The initial concentration of colloidal species within the drying drop (or film) also plays an important role in pattern formation. In the dilute limit, colloidal particles segregate into discrete patterned features with a final height (h_f) as small as several micrometres and lateral dimensions of the order of the hole diameter, d_h. However, as the colloid volume fraction increases, there is a transition from discrete patterned features to continuously patterned films. This transition takes place when the diameter of the patterned features d_f is equal to the pitch P, which occurs when the initial microsphere volume fraction ϕ_μ exceeds a critical value ϕ_μ^*. When $\phi_\mu \gg \phi_\mu^*$, even thicker films are formed that possess a patterned surface topography. To determine ϕ_μ^* or the mask design shown in figure 1*a*, we set $d_f = P$ and equate the total initial microsphere volume within a hexagonal region around each open feature, $V_i = \phi_\mu (P^2\sqrt{3}/2)h_i$, to the final microsphere volume within each patterned hemi-ellipsoidal feature, $V_f = \phi_f \pi\, d_f^3/600$, where h_i is the initial film height ($\approx 100\,\mu$m). We assume that $\phi_f = 0.64$, which corresponds to the random close-packed volume fraction for monodisperse spheres, and use the experimentally determined value of $h_f/d_f \approx 0.02$ (Harris *et al.* 2007). For unary films dried under a mask with a periodic array of holes ($d_h = 250\,\mu$m, $P = 5d_h$), we find that $\phi_\mu^* \approx \pi\phi_f P/300\sqrt{3}h_i \approx 0.05$. Below, we demonstrate how this transition can be exploited in binary mixtures to preferentially segregate one species in a continuous film of another, as illustrated in figure 1*c*.

3. Pattern formation in binary colloidal films

To explore evaporative lithographic patterning of binary colloidal mixtures, we first created an aqueous suspension of silica microspheres and sulphonated polystyrene nanoparticles with respective volume fractions of $\phi_\mu = 0.3$ and $\phi_{nano} = 10^{-3}$ and particle radii of $a_m = 0.59\,\mu$m and $a_n = 10\,$nm. Figure 3 shows a patterned film that was prepared under a mask with $d_h = 250\,\mu$m, $P = 5d_h$ and $h_g \approx 30\,\mu$m. These particle volume fractions were purposely chosen such that $\phi_\mu > \phi^*$ and $\phi_{nano} \ll \phi^*$, where $\phi^* \sim 0.05$ for this mask design, as discussed in §2. Under these conditions, the microspheres quickly consolidate to form a continuous patterned film, while the nanoparticles remain entrained in the fluid and segregate to the regions of highest evaporative flux yielding discretely patterned features. The surface topography of the dried binary films shown in figure 3*a* is analogous to that observed for unary colloidal films at identical ϕ_μ. To determine the extent of nanoparticle segregation, we imbibed the patterned binary film with a dimethylsulphoxide (DMSO) : water solution that matched the refractive index of the silica microspheres. The refractive index mismatch between the imbibed solution and the polystyrene nanoparticles allowed direct visualization of their distribution (figure 3*b*). The magnified view of a nanoparticle-rich feature provided in figure 3*c* reveals a diameter of approximately $250\,\mu$m, which is roughly equivalent to the hole size d_h within the mask.

Varying the mask design alters the evaporative landscape above the drying film, and, hence, the resulting patterns are formed. Figure 4*a–f* shows a series of fluorescence images acquired for binary films dried under masks with varying d_h and P at a constant $h_g \approx 30\,\mu$m. These films were produced from binary suspensions initially composed of $\phi_\mu = 0.3$ and $\phi_{nano} = 10^{-3}$ and particle

radii of $a_m = 0.59\,\mu m$ and $a_n = 10\,nm$, which were dried beneath masks of $d_h = 250$ or $500\,\mu m$ and $P = 2$, 5 or $10 d_h$. Again, the microspheres form a continuous patterned film, similar to that observed in figure 3*a*, whose surface topography varies with d_h and P. In this set of experiments, fluorescently labelled nanoparticles were used to both circumvent the need to imbibe the DMSO : water solution and enhance the resolution of the imaged features. The fluorescence micrographs clearly show that nanoparticles segregate laterally to yield a periodic array of discrete, nanoparticle-rich features embedded within the continuous microsphere films.

In the initial stage of drying, silica microspheres and polystyrene nanoparticles are transported to regions of high evaporative flux by particle convection. As drying proceeds, the microspheres consolidate into a close-packed network that contains interstitial pores of radius $a_p \approx 0.15\, a_\mu$. Since $\phi_\mu \sim 0.5\,\phi_f$, this transition occurs when roughly 50 per cent of the water has evaporated from the film. Because $\phi_{nano} \ll \phi^* < \phi_f$, the nanoparticles remain entrained in the liquid well beyond this point; moreover, since $a_{nano} \ll a_p$, they are able to migrate through the porous microsphere network. As the drying front recedes into the film, capillary tension at the liquid menisci creates a pressure gradient, $P_c = -2\gamma_{lv}/a_p$, that further enhances nanoparticle segregation, where γ_{lv} is the liquid–vapour surface tension. Using the measured surface tension of $27\,mNm^{-1}$, the calculated pressure drop is approximately -6 atm.

To investigate the effects of the particle size ratio on pattern formation, we prepared a series of binary colloidal suspensions of fixed $\phi_\mu = 0.3$ and $\phi_{nano} = 10^{-3}$, but varying a_μ/a_{nano}. The films were dried under a mask with d_h=250 μm, P=5d_h and $h_g \approx 30\,\mu m$. Figure 5 shows the fluorescence images of the dried films; the diameter of the patterned features increased as a_μ/a_{nano} decreased. The extent of nanoparticle segregation is quantified by plotting the diameter of the patterned features as a function of a_μ/a_{nano} (figure 6). When $a_\mu/a_{nano} > 7$, significant nanoparticle segregation occurs and the diameter of the observed patterned features is comparable to d_h, as shown in figure 6. At a critical value of $a_\mu/a_{nano} \sim 7$, the nanoparticle size is now equivalent to the characteristic pore size, i.e. $a_{nano} = a_p \approx 0.15 a_\mu$. When $a_\mu/a_{nano} \leq 7$, there is an abrupt change in feature size as the transport of nanoparticles within this porous network becomes hindered. In actuality, the microsphere network contains a distribution of pore sizes, hence some nanoparticle segregation persists even when $a_{nano} > a_p$. Not surprisingly, as a_μ/a_{nano} decreases even further, there is a concomitant rise in the size of the patterned, nanoparticle-rich features. Ultimately, when $a_\mu/a_{nano} \approx 1$, the features are comparable in size to the pitch P, indicating that pattern formation has been effectively suppressed.

4. Conclusions

Evaporative lithographic patterning offers many advantages over other assembly routes, including its simplicity and the ability to control particle deposition without substrate modification. Importantly, it provides a promising new avenue for patterning soft materials, including colloidal, polymeric and biomolecular species. Our investigation, albeit confined to a narrow compositional window, demonstrates that evaporative lithography can be readily extended to binary

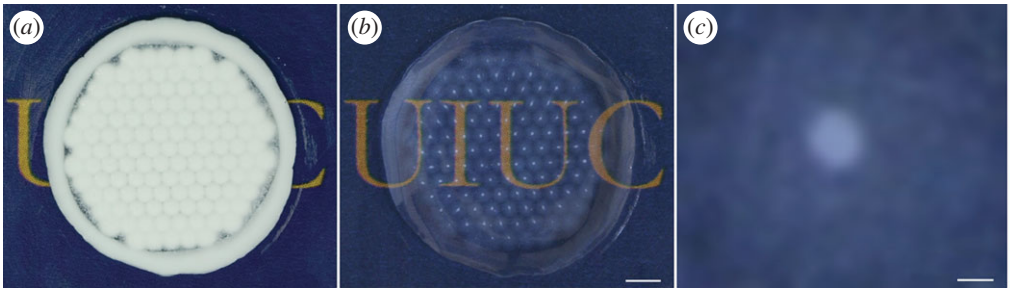

Figure 3. Optical images of a patterned microsphere–nanoparticle film dried under a mask with $d_h = 250\,\mu m$ and $P = 5d_h$. (*a*) Only the microspheres are visible in the dried film. (*b*) After imbibing the film with an index matching DMSO : water solution, the silica film becomes transparent, leaving the polystyrene nanoparticles clearly visible (scale bar: 5 mm). (*c*) A magnified view of a single nanoparticle feature shows the lateral segregation of the nanoparticles (scale bar: 250 μm).

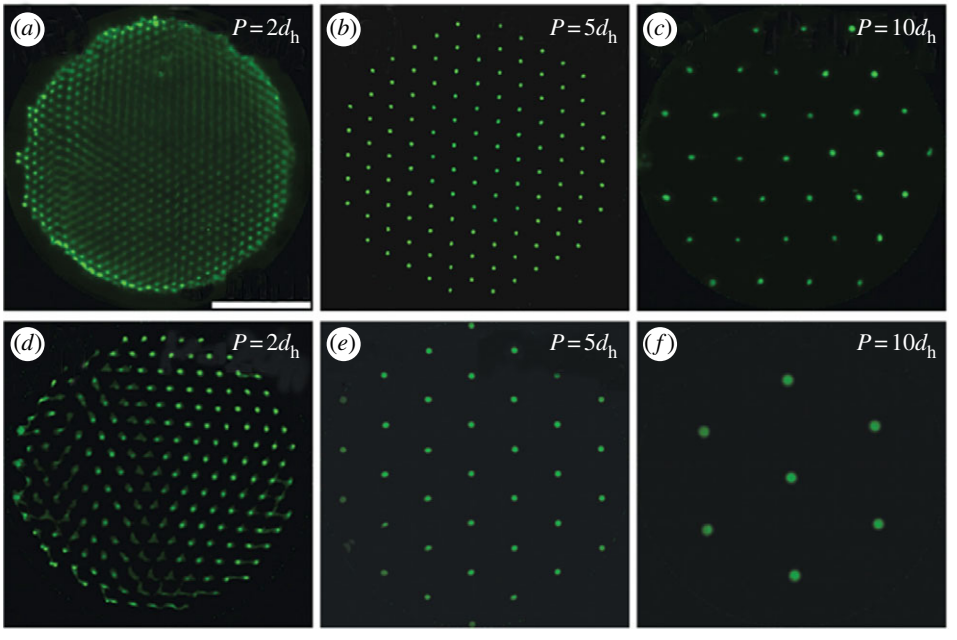

Figure 4. Fluorescence images of patterned binary films dried under masks with $d_h = 250\,\mu m$ (*a–c*) or 500 μm (*d–f*) and varying centre-to-centre distance between holes, P, of 2, 5 or $10d_h$, in which only the fluorescent nanoparticles are shown. Scale bar: 5 mm. Adapted from Harris *et al.* (2007).

mixtures. Looking towards the future, we anticipate that a rich array of patterned films can be produced by varying the respective microsphere and nanoparticle concentrations and exploring non-aqueous systems.

This work is based on research supported by the National Science Foundation (grant no. DMR-0652424). The authors gratefully acknowledge the contributions of H. Hu (Proctor and Gamble), who carried out FEM analysis, and W. Wu, who assisted with figure preparation.

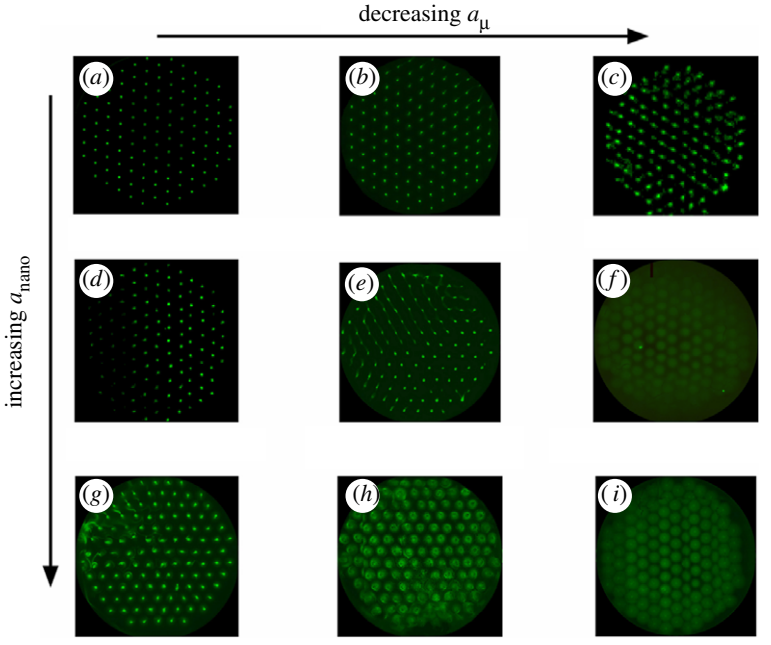

Figure 5. Fluorescence images of binary colloidal films prepared from suspensions of constant $\phi_\mu = 0.3$, $\phi_{nano} = 10^{-3}$ and varying a_μ/a_{nano}, in which only the fluorescent nanoparticles are shown. The films were dried under masks with $d_h = 250\,\mu m$, $P = 5d_h$ and $h_g \approx 30\,\mu m$. (*a*) $a_{micro}/a_{nano} = 47$, (*b*) $a_{micro}/a_{nano} = 25$, (*c*) $a_{micro}/a_{nano} = 10.6$, (*d*) $a_{micro}/a_{nano} = 15.8$, (*e*) $a_{micro}/a_{nano} = 8.3$, (*f*) $a_{micro}/a_{nano} = 3.5$, (*g*) $a_{micro}/a_{nano} = 4.7$, (*h*) $a_{micro}/a_{nano} = 2.5$ and (*i*) $a_{micro}/a_{nano} = 1.1$.

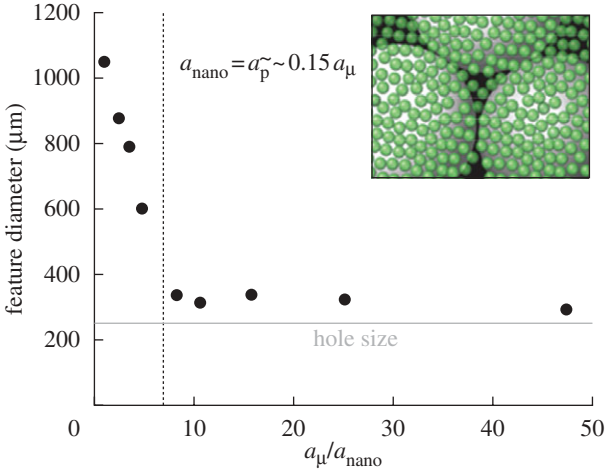

Figure 6. Plot of the patterned feature diameter as a function of a_μ/a_{nano} for films assembled from binary suspensions of fixed $\phi_\mu = 0.3$ and $\phi_{nano} = 10^{-3}$, but varying size ratio, a_μ/a_{nano}. The films were dried under a mask with $d_h = 250\,\mu m$ and $P = 5d_h$. (Note: inset depicts the interstitial pores formed between close-packed microspheres and surrounding nanoparticles in binary mixtures of high size ratio.)

References

Aizenberg, J., Braun, P. V. & Wiltzius, P. 2000 Patterned colloidal deposition controlled by electrostatic and capillary forces. *Phys. Rev. Lett.* **84**, 2997–3000. (doi:10.1103/PhysRevLett.84.2997)

Berg, J. C., Boudart, M. & Acrivos, A. J. 1966 Natural convection in pools of evaporating liquids. *J. Fluid Mech.* **24**, 721–735. (doi:10.1017/S0022112066000958)

Bhatt, K. H., Grego, S. & Velev, O. D. 2005 An AC electrokinetic technique for collection and concentration of particles and cells on patterned electrodes. *Langmuir* **21**, 6603–6612. (doi:10.1021/la050658w)

Chiu, R. C. & Cima, M. J. 1993 Drying of granular ceramic films: II, drying stress and saturation uniformity. *J. Am. Ceram. Soc.* **76**, 2769–2777. (doi:10.1111/j.1151-2916.1993.tb04014.x)

Deegan, R. D. 2000 Pattern formation in drying drops. *Phys. Rev. E* **61**, 475–485. (doi:10.1103/PhysRevE.61.475)

Deegan, R. D., Bakajin, O., Dupont, T. F., Huber, G., Nagel, S. R. & Witten, T. A. 1997 Capillary flow as the cause of ring stains from dried liquid drops. *Nature* **389**, 827–829. (doi:10.1038/39827)

Deegan, R. D., Bakajin, O., Dupont, T. F., Huber, G., Nagel, S. R. & Witten, T. A. 2000 Contact line deposits in an evaporating drop. *Phys. Rev. E* **62**, 756–765. (doi:10.1103/PhysRevE.62.756)

Girard, F., Antoni, M., Faure, S. & Steinchen, A. 2006 Evaporation and Marangoni driven convection in small heated water droplets. *Langmuir* **22**, 11 085–11 091. (doi:10.1021/la061572l)

Harris, D. J. & Lewis, J. A. 2008 Marangoni effects on evaporative lithographic patterning of colloidal films. *Langmuir* **24**, 3682–3685. (doi:10.1021/la8000637)

Harris, D. J., Hu, H., Conrad, J. C. & Lewis, J. A. 2007 Patterning colloidal films via evaporative lithography. *Phys. Rev. Lett.* **98**, 148301. (doi:10.1103/PhysRevLett.98.148301)

Hayward, R. C., Saville, D. A. & Aksay, I. A. 2000 Electrophoretic assembly of colloidal crystals with optically tunable micropatterns. *Nature* **404**, 56–59. (doi:10.1038/35003530)

Hu, H. & Larson, R. G. 2005*a* Analysis of the microfluidic flow in an evaporating sessile droplet. *Langmuir* **21**, 3963–3971. (doi:10.1021/la047528s)

Hu, H. & Larson, R. G. 2005*b* Analysis of the effects of Marangoni stresses on the microflow in an evaporating sessile droplet. *Langmuir* **21**, 3972–3980. (doi:10.1021/la0475270)

Hu, H. & Larson, R. G. 2006 Marangoni effect reverses coffee-ring depositions. *J. Phys. Chem. B* **110**, 7090–7094. (doi:10.1021/jp0609232)

Jing, J. *et al.* 1998 Automated high resolution optical mapping using arrayed, fluid-fixed DNA molecules. *Proc. Natl Acad. Sci. USA* **95**, 8046–8051. (doi:10.1073/pnas.95.14.8046)

Lee, I., Zheng, H., Rubner, M. F. & Hammond, P. T. 2002 Controlled cluster size in patterned particle arrays via directed adsorption on confined surfaces. *Adv. Mater.* **14**, 572–577. (doi:10.1002/1521-4095(20020418)14:8<572::AID-ADMA572>3.0.CO;2-B)

Lee, W., Chan, A. T., Bevan, M. A., Lewis, J. A. & Braun, P. V. 2004 Nanoparticle-mediated epitaxial assembly of colloidal crystals on patterned substrates. *Langmuir* **20**, 5262–5670. (doi:10.1021/la035694e)

Lin, K. H., Crocker, J. C., Prasad, V., Schofield, A., Weitz, D. A., Lubensky, T. C. & Yodh, A. G. 2000 Entropically driven colloidal crystallization on patterned surfaces. *Phys. Rev. Lett.* **85**, 1770–1773. (doi:10.1103/PhysRevLett.85.1770)

Martinez, C. J. & Lewis, J. A. 2002 Shape evolution and stress development during latex-silica film formation. *Langmuir* **18**, 4689–4698. (doi:10.1021/la0114833)

Masuda, Y., Koumura, T., Okawa, T. & Koumoto, K. 2003 Micropatterning of Ni particles on a $BaTiO_3$ green sheet using a self-assembled monolayer. *J. Colloid Interface Sci.* **263**, 190–195. (doi:10.1016/S0021-9797(03)00217-0)

Richetti, P., Prost, J. & Barois, P. 1984 Two-dimensional aggregation and crystallization of a colloidal suspension of latex spheres. *J. Phys. Lett.* (*Paris*) **45**, 1137–1143. (doi:10.1051/jphyslet:0198400450230113700)

Ristenpart, W. D., Aksay, I. A. & Saville, D. A. 2003 Electrically guided assembly of planar superlattices in binary colloidal suspensions. *Phys. Rev. Lett.* **90**, 128303. (doi:10.1103/PhysRevLett.90.128303)

Ristenpart, W. D., Aksay, I. A. & Saville, D. A. 2004 Assembly of colloidal aggregates by electrohydrodynamic flow: kinetic experiments and scaling analysis. *Phys. Rev. E* **69**, 021405. (doi:10.1103/PhysRevE.69.021405)

Ristenpart, W. D., Kim, P. G., Domingues, C., Wan, J. & Stone, H. A. 2007 Influence of substrate conductivity on circulation reversal in evaporating drops. *Phys. Rev. Lett.* **99**, 234502. (doi:10.1103/PhysRevLett.99.234502)

Routh, A. F. & Russel, W. B. 1998 Horizontal drying fronts during solvent evaporation from latex films. *AIChE J.* **44**, 2088–2098. (doi:10.1002/aic.690440916)

Savino, R., Paterna, D. & Favaloro, N. 2002 Buoyancy and Marangoni effects in an evaporating drop. *J. Thermophys. Heat Tr.* **16**, 562–574.

Shmuylovich, L., Shen, A. Q. & Stone, H. A. 2002 Surface morphology of drying latex films: multiple ring formation. *Langmuir* **18**, 3441–3445. (doi:10.1021/la011484v)

Smalyukh, I. I., Zribi, O. V., Butler, J. C., Lavrentovich, O. D. & Wong, G. C. L. 2006 Structure and dynamics of liquid crystalline pattern formation in drying droplets of DNA. *Phys. Rev. Lett.* **96**, 177801. (doi:10.1103/PhysRevLett.96.177801)

van Blaaderen, A., Ruel, R. & Wiltzius, P. 1997 Template-directed colloidal crystallization. *Nature* **385**, 321–324. (doi:10.1038/385321a0)

Velev, O. D. & Bhatt, K. H. 2006 On-chip micromanipulation and assembly of colloidal particles by electric fields. *Soft Matter* **2**, 738–750. (doi:10.1039/b605052b)

Yin, Y., Lu, Y., Gates, B. & Xia, Y. 2001 Template-assisted self-assembly: a practical route to complex aggregates of monodispersed colloids with well-defined sizes, shapes, and structures. *J. Am. Chem. Soc.* **123**, 8718–8729. (doi:10.1021/ja011048v)

Zheng, H., Lee, I., Rubner, M. F. & Hammond, P. T. 2002 Two component particle arrays on patterned polyelectrolyte multilayer templates. *Adv. Mater.* **14**, 569–572. (doi:10.1002/1521-4095(20020418)14:8<569::AID-ADMA569>3.0.CO;2-O)